Density Functional Calculations of *g*-Tensors of Low-Spin Iron(I) and Iron(III) Porphyrins

E. van Lenthe*,† and A. van der Avoird

Institute of Theoretical Chemistry, NSR Center, University of Nijmegen, Toernooiveld, 6525 ED Nijmegen, The Netherlands

W. R. Hagen and E. J. Reijerse

Department of Molecular Spectroscopy, NSR Center, University of Nijmegen, Toernooiveld, 6525 ED Nijmegen, The Netherlands

Received: August 20, 1999; In Final Form: December 7, 1999

The *g*-values of some selected low-spin Fe(I) and Fe(III) porphyrin complexes have been calculated, using a method based on density functional theory and the zeroth order regular approximation to the Dirac equation. In agreement with experimental observations the calculated *g*-values of these complexes differ strongly from the free electron g_e-value. Optimization of the geometries gives iron−ligand distances in good agreement with the experimentally derived values. The effects of strong ruffling of the porphyrin core and of the relative orientation of the planes of axial ligands on the *g*-values are evaluated quantitatively. Mechanisms reported for these effects are confirmed.

I. Introduction

Iron porphyrins play an important role in the cells of many living organisms. It is therefore not surprising that such complexes have been studied extensively, both experimentally and theoretically. If the iron porphyrin is paramagnetic it can be investigated by electron paramagnetic resonance (EPR) spectroscopy. Low-spin Fe(III) porphyrins are of special interest because much can be learned about the nature of the unpaired electron. Other techniques are also used often to study the paramagnetic states of iron, such as NMR and Mössbauer spectroscopy. In this article we calculate the *g*-values for low-spin iron(I) and iron(III) porphyrins with the use of a recently developed method,[1] which applies density functional theory and spin−orbit coupled equations. The experimental EPR *g*-values of low-spin Fe(III) porphyrins are often analyzed with a relatively simple model by Taylor,[2] in which the orbital of the unpaired electron is composed only of the iron d_{xz}, d_{yz}, and d_{xy} orbitals. We will analyze the calculated unpaired electron orbital in a similar way, and compare the results with Taylor's model.

Different theoretical approaches have been used to understand the electronic structure and molecular geometries of iron porphyrins, for example Extended Hückel calculations,[3,4] ab initio calculations,[5,6] density functional theory,[7−9] molecular mechanics,[10] and Car−Parrinello molecular dynamics.[11] Our approach uses density functional theory, with nonrelativistic density functionals for the exchange-correlation energy. For our spin−orbit coupled equations we use the zeroth order regular approximation (ZORA)[12−15] to the Dirac equation.

In this article we investigate the 4-coordinate (no axial ligand) low-spin Fe(I) porphyrin $[(P)Fe]^-$ and the 6-coordinate (two axial ligands) low-spin Fe(III) porphyrins $[(P)Fe(ImH)_2]^+$, $[(P)Fe(Pz)_2]^+$, and $[(P)Fe(Py)_2]^+$ (see footnote *a* of Table 1 for abbreviations). These complexes were chosen because their experimental *g*-values differ significantly from the free electron g_e-value. On the other hand, these complexes are still small enough to apply our recently developed method[1] for the calculation of *g*-values. Geometry optimizations have been performed on all complexes, and the calculated structures are compared with appropriate X-ray structures. The structures of the calculated compounds are drawn schematically in Figure 1.

TABLE 1: Calculated *g*-Values of $[(P)Fe]^-$ from ZORA Spin Restricted Frozen Core Calculations and Calculated Percentages of the Iron d Orbital Contributions to the Unpaired Electron[a]

	sign of $g_xg_yg_z$	g_x	g_y	g_z	$(d_{z^2})^b$	$(d_{xz})^b$	$(d_{yz})^b$
AOC	+	2.51	2.51	2.01	96.5	1.7	1.7
SCF	+	3.02	3.02	1.85	78.6	10.7	10.7
experiment[37]							
$[(TPP)Fe]^-$		2.3	2.3	1.93	96.5	0.3	0.3
$[(OEP)Fe]^-$		2.24	2.24	1.92	96.0	0.2	0.2

[a] Abbreviations: P, porphyrin; ImH, imidazole; Pz, pyrazole; Py, pyridine; (TPP)Fe, iron tetraphenylporphyrin; (OEP)Fe, iron octaethylporphyrin; (TMP)Fe, iron tetramesitylporphyrin; (PP)Fe, iron protoporphyrin IX. [b] See the text for the exact meaning of these percentages.

Many experimental and some theoretical investigations of the relative orientation of planar ligands in low-spin iron (III) porphyrins, and of the effects of these orientations on the observed spectra have been performed. (See, for example, Refs 10, 16−21). In this study we also investigate these ligand orientation effects, especially on the calculated *g*-values.

II. The Effective Spin Hamiltonian

In Ref 1 a method was developed for the calculation of the *g*-tensor of Kramers doublet open-shell molecules, which uses the spinor of the unpaired electron of the paramagnetic molecule obtained from a density functional calculation. Spin−orbit coupling was taken into account variationally using the ZORA equation. In this section we repeat some of the main aspects of this method.

† Present address: Afdeling Theoretische Chemie, Vrije Universiteit, De Boelelaan 1083, 1081 HV Amsterdam, The Netherlands.

10.1021/jp992959i CCC: $19.00
Published on Web 02/23/2000

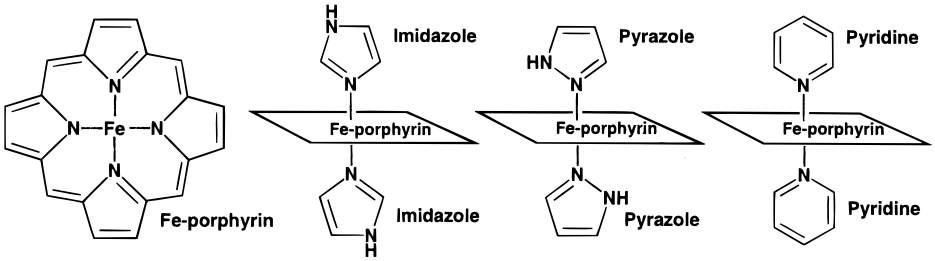

Figure 1. Schematic view of the calculated low-spin iron−porphyrin complexes $[(P)Fe]^-$, $[(P)Fe(ImH)_2]^+$, $[(P)Fe(Pz)_2]^+$, and $[(P)Fe(Py)_2]^+$, respectively.

For a paramagnetic molecule in an external homogeneous magnetic field $\boldsymbol{B}^0$, the electronic Zeeman interaction H^Z may be written effectively as (in a.u.):

$$H^Z = \boldsymbol{B}^0 \cdot \frac{\boldsymbol{g}}{2c} \cdot \tilde{\boldsymbol{S}} \tag{1}$$

The molecular *g*-tensor parametrizes the interaction between the effective spin $\tilde{\boldsymbol{S}}$ of the molecule and the external magnetic field.

We consider only one-electron equations in our theoretical approach, because we use density functional theory. The effective Kohn−Sham potential *V* in our formalism is the sum of the nuclear potential, the Coulomb potential caused by the total electron density, and the exchange-correlation potential, for which we use nonrelativistic approximations.

The ZORA equation for a negatively charged particle in an electromagnetic field can be written in atomic units ($\boldsymbol{p} = -i\nabla$) as[1]:

$$\left(V + \boldsymbol{\sigma}\cdot\boldsymbol{\Pi}\frac{K}{2}\boldsymbol{\sigma}\cdot\boldsymbol{\Pi}\right)\Psi^{\text{zora}} = E^{\text{zora}}\Psi^{\text{zora}} \tag{2}$$

with

$$\boldsymbol{\Pi} = \boldsymbol{p} + \frac{\boldsymbol{A}^0}{c} \tag{3}$$

In these equations $K = [1 - V/2c^2]^{-1}$, $\boldsymbol{\sigma}$ are the Pauli spin matrixes, *c* is the velocity of light, $\boldsymbol{B}^0 = \nabla \times \boldsymbol{A}^0$ is the magnetic field, and $\boldsymbol{A}^0$ is the vector potential associated with this field. We will explicitly substitute the $-i\nabla$ form for $\boldsymbol{p}$ when the gradient only works on the function next to it.

The terms linear in the field in eq 2 form the Zeeman Hamiltonian:

$$H^Z = \frac{g_e}{2c}\left[\frac{K}{2}\boldsymbol{\sigma}\cdot\boldsymbol{B}^0 + \frac{K}{4}\boldsymbol{B}^0\cdot\boldsymbol{L} + \boldsymbol{B}^0\cdot\boldsymbol{L}\frac{K}{4} + \boldsymbol{\sigma}\cdot\left(\nabla\frac{K}{2}\times\boldsymbol{A}^0\right)\right], \tag{4}$$

$\boldsymbol{L} = \boldsymbol{r} \times \boldsymbol{p}$ is the orbital angular momentum operator. A factor $g_e/2$ was included to account for quantum electrodynamic effects in the $\boldsymbol{\sigma}\cdot\boldsymbol{B}^0$ term. For convenience this factor $g_e/2$, which is very close to unity, was also included in all the other terms that are linear in $\boldsymbol{A}^0$.

We assume that we have an odd number of electrons in the paramagnetic molecule and that the ground level has only Kramers degeneracy. The "spin Hamiltonian" of such a Kramers doublet was discussed by Abragam and Bleaney.[22] Just as in Ref 1 we follow this discussion, assuming that this doublet completely determines this spin Hamiltonian. Hence, we only need to calculate the matrix elements of the Zeeman Hamiltonian between the two degenerate spinors Φ_1 and Φ_2, which are eigenfunctions of the ZORA equation without a magnetic field. These two spinors, which are connected by time-reversal symmetry, may be written as

$$\Phi_1 = \begin{pmatrix}\phi_a\\ \phi_b\end{pmatrix} \qquad \Phi_2 = \begin{pmatrix}-\phi_b^*\\ \phi_a^*\end{pmatrix} \tag{5}$$

and for the energy in first order in the magnetic field we obtain the following equations:

$$\frac{\partial}{\partial B_k^0}\begin{pmatrix}\langle\Phi_1|H^Z|\Phi_1\rangle & \langle\Phi_1|H^Z|\Phi_2\rangle\\ \langle\Phi_2|H^Z|\Phi_1\rangle & \langle\Phi_2|H^Z|\Phi_2\rangle\end{pmatrix} = \frac{1}{4c}\sum_l g_{kl}\sigma_l \tag{6}$$

with real coefficients g_{kl}. The g_{kl} are calculated as

$$g_{kx} = 4c\ \mathrm{Re}\left\langle\Phi_1\left|\frac{\partial}{\partial B_k^0}H^Z\right|\Phi_2\right\rangle \tag{7a}$$

$$g_{ky} = -4c\ \mathrm{Im}\left\langle\Phi_1\left|\frac{\partial}{\partial B_k^0}H^Z\right|\Phi_2\right\rangle \tag{7b}$$

$$g_{kz} = -4c\ \mathrm{Re}\left\langle\Phi_1\left|\frac{\partial}{\partial B_k^0}H^Z\right|\Phi_1\right\rangle \tag{7c}$$

and from the real numbers g_{kl} one can construct a true tensor:

$$G_{pq} = \sum_k g_{pk}g_{qk} \tag{8}$$

This tensor can be diagonalized by a proper choice of coordinate axes. The eigenvalues of this matrix are the squares of the *g*-values. Just as in the experiment we can only obtain the absolute *g*-values, although the sign of the product of the three *g*-values can still be calculated (and measured), because the determinant of the matrix g_{kl} is invariant under spatial rotations, and under mixing of the two degenerate spinors.[22]

In the preceding text, it is assumed that the two degenerate spinors of the unpaired electron completely determine the magnetic Hamiltonian. This is true in spin-restricted density functional theory. Without magnetic field in our density functional calculations we obtain two degenerate wave functions, which are Slater determinants, connected to each other by time-reversal symmetry. In the spin-restricted case the spinors of the 'paired' electrons in these Slater determinants are also connected to each other by time-reversal symmetry. Because both are occupied, they give zero contribution to the matrix elements of the magnetic Hamiltonian in first order. Therefore, the only nonzero contribution originates from the two degenerate spinors of the unpaired electron.

Reference 1 presents details about how the problem of gauge dependence was solved by using gauge including atomic orbitals (GIAOs) and how the scaled ZORA energy expression was included in the evaluation of the *g*-values. These effects are included in the calculated *g*-values presented in this article. The

scaled ZORA energy expression only gives a very small correction to the ZORA *g*-values.

III. Computational Details

The Amsterdam Density Functional (ADF) program[23,24] was applied in the calculations. This program performs self-consistent field calculations using density functional theory (DFT), solving the one-electron Kohn−Sham equations. We used the local density functional (LDA) parametrized by Vosko et al.,[25] with gradient correction (BP) terms added, namely the Becke correction for exchange[26] and the Perdew correction for correlation,[27] in its spin-restricted form.

In all our calculations we used the point group symmetry of the molecule. Double group symmetry adapted functions were used when spin−orbit coupling was included, in the ZORA case. For more details concerning the implementation of ZORA in ADF, see Refs 28 and 29 and references therein. A triple-ζ valence Slater-type orbital (STO) basis set plus two polarization functions were used for iron, the porphyrin nitrogens, and the atom in the ligand(s) which is closest to iron. All other atoms were represented with a double-ζ valence STO basis set. The frozen core approximation was used, with the 1s, 2s, and 2p of Fe and the 1s of C and N assigned to the core.

We performed ZORA scalar relativistic (no spin−orbit coupling) geometry optimizations on the low-spin iron porphyrin [(P)Fe] complexes. We calculated the 4-coordinate (no axial ligand) low-spin Fe(I) porphyrin [(P)Fe]- and the 6-coordinate (two axial ligands) low-spin Fe(III) porphyrins $[(P)Fe(ImH)_2]^+$, $[(P)Fe(Pz)_2]^+$, and $[(P)Fe(Py)_2]^+$ (see footnote *a* Table 1 for abbreviations). The structures of the calculated iron−porphyrin complexes are drawn schematically in Figure 1.

These calculated complexes are open-shell molecules, which all have one electron less than a closed-shell configuration. We chose to distribute the corresponding hole equally over the nearly degenerate orbitals present in the calculation, using fractional occupation numbers. This means that we calculate an average of configuration (AOC) of nearly degenerate states. This procedure was helpful in the convergence of the geometry optimization. The ZORA scalar relativistic optimized geometries are used in the ZORA spin−orbit coupled equations (ZORA SCF). In these spin−orbit coupled equations we use integer occupation numbers, because our method for the evaluation of the *g*-tensor[1] requires a one-determinantal (pure state) wave function. In the ZORA AOC calculation the scalar relativistic AOC electron density is used for the evaluation of the Kohn−Sham potential, whereas in the ZORA SCF calculation the spin−orbit coupled equation is solved self-consistently.

We investigate the influence on the calculated *g*-tensor of the orientation of the axial ligand(s) with respect to the porphyrin. The axes are chosen such that the iron porphyrin always lies in the *xy*-plane. The axial planar ligands, if present, always lie perpendicular to the plane of the porphyrin. If two mutually perpendicular planar axial ligands are present, the *x*- and *y*-axes are chosen to bisect the planes of these axial ligands. If two mutually parallel axial planar ligands are present, these axial ligands lie in the *xz*-plane.

IV. Results and Discussion

Four-Coordinate Low-Spin Fe(I) Porphyrin $[(P)Fe]^-$. A scalar relativistic geometry optimization was performed for $[(P)Fe]^-$ in D_{4h} symmetry. The optimized FeN_p distance, with N_p a porphyrin nitrogen, in the AOC calculation was 1.97 Å. We chose to distribute the unpaired electron hole equally over the nearly degenerate orbitals a_{1g} (approximately 85% iron d_{z^2} character), b_{2g} (95% d_{xy}), and e_g (65% d_{xz} and d_{yz}), using the fractional occupation numbers 1/4, 1/4, and 1/2. This means that we calculate an AOC of the nearly degenerate A_{1g}, B_{2g}, and E_g states. The ground state in the scalar relativistic calculation is the A_{1g} state, because the a_{1g} orbital has the highest orbital energy. This A_{1g} state can be written approximately as $(d_{xy})^2(d_{xz},d_{yz})^4\ (d_{z^2})^1$. In the spin−orbit coupled equation the unpaired electron has mainly a_{1g} character with a little mixing of e_g character. In Table 1 we present the calculated *g*-values. The percentages given in this table correspond to the calculated total a_{1g} and e_g character of the unpaired electron, thus not only the part that is due to the iron d orbitals.

If the Kramers pair could be written as

$$\Phi_1 = \begin{pmatrix} a d_{z^2} \\ -b d_{xz} - i b d_{yz} \end{pmatrix} \qquad \Phi_2 = \begin{pmatrix} b d_{xz} - i b d_{yz} \\ a d_{z^2} \end{pmatrix} \tag{9}$$

with real coefficients *a* and *b*, the *g*-values would be

$$g_{\parallel} = 2a^2 \tag{10a}$$

$$g_{\perp} = 2a^2 + 4\sqrt{3}ab \tag{10b}$$

A more involved model can be found in the theoretical work of McGarvey on Co(II),[30] for example. We find that the spinors do not consist purely of the iron d orbitals, which means that eq 10 is only approximately valid. In the AOC calculation we find $a \approx 0.9$, $b \approx 0.1$, and in the SCF calculation $a \approx 0.8$, $b \approx 0.25$. If we use these numbers to calculate the difference $g_{\perp} - g_{\parallel} = 4\sqrt{3}ab$ according to eq 10, we find that this relation gives a value that is slightly too large compared with the actual difference in Table 1. If we assume that the relation for the difference also holds approximately for the experimental *g*-values, we find that *b* should be on the order of 0.05 to explain the experiment. The experimental iron d orbital contributions given in Table 1 are calculated from the experimental *g*-values as the squares of the coefficients *a* and *b* in eq 9 times 100%. We may expect better agreement with the experiment if the d_{xz} and d_{yz} character of the unpaired electron in our calculation decreases.

Six-Coordinate Low-Spin Fe(III) Porphyrins. A simple and very useful model by Taylor[2] describes the Kramers pair of low-spin Fe(III) porphyrins in terms of the iron d_{xy}, d_{xz}, and d_{yz} orbitals:

$$\Phi_1 = \begin{pmatrix} a d_{yz} - i b d_{xz} \\ -c d_{xy} \end{pmatrix} \qquad \Phi_2 = \begin{pmatrix} c d_{xy} \\ a d_{yz} + i b d_{xz} \end{pmatrix} \tag{11}$$

The *g*-values can then be calculated as

$$g_x = 2[a^2 - (b + c)^2] \tag{12a}$$

$$g_y = 2[(a + c)^2 - b^2] \tag{12b}$$

$$g_z = 2[(a + b)^2 - c^2] \tag{12c}$$

By inversion of these equations one obtains

$$a = \frac{(g_y + g_z)}{\sqrt{8(g_z + g_y - g_x)}} \tag{13a}$$

$$b = \frac{(g_z - g_x)}{\sqrt{8(g_z + g_y - g_x)}} \tag{13b}$$

$$c = \frac{(g_y - g_x)}{\sqrt{8(g_z + g_y - g_x)}} \tag{13c}$$

These relations are frequently used to characterize the unpaired electron from the experimental *g*-values. Also the signs of the *g*-values are needed for this purpose. However, in EPR experiments one often only measures g^2. As explained, for example, by Abragam and Bleaney,[22] the only meaningful sign is the sign of the product $g_x g_y g_z$, which can be determined if one uses circularly polarized radiation. The remaining signs are arbitrary. For a given sign of the product $g_x g_y g_z$, it is always possible to choose the signs of the *g*-values such that $g_z + g_y - g_x$ is positive, which is needed in Taylor's model.[2] The experimental values of the iron d orbital contributions listed in Tables 2 to 4 are calculated according to this model as the squares of the coefficients in eq 13 times 100%. On the other hand, the percentages of the iron d orbital contributions from our DFT calculations correspond to the calculated d character of the unpaired electron, but also include all other contributions that have the same symmetry as the particular d orbital. In this way we ensure that the sum of the percentages in our DFT calculations is 100%.

The *g*-tensor of the unpaired electron in our calculations is given approximately by eq 12 if the plane of the (mutually parallel) axial ligands lies over the porphyrin nitrogens, or if two mutually perpendicular axial ligands lie over the meso position of the porphyrin ring. However, if the plane of the (mutually parallel) axial ligands lies over the meso position of the porphyrin ring, or if two mutually perpendicular axial ligands lie over the porphyrin nitrogens, the unpaired electron can be described better by

$$\Phi_1 = \begin{pmatrix} a\mathrm{d}_{yz} - ib\mathrm{d}_{xz} \\ ic\mathrm{d}_{x^2-y^2} \end{pmatrix} \qquad \Phi_2 = \begin{pmatrix} ic\mathrm{d}_{x^2-y^2} \\ a\mathrm{d}_{yz} - ib\mathrm{d}_{xz} \end{pmatrix} \tag{14}$$

In this case the *g*-values are:

$$g_x = 2[(a + c)^2 - b^2] \tag{15a}$$

$$g_y = 2[a^2 - (b + c)^2] \tag{15b}$$

$$g_x = 2[(a + b)^2 - c^2] \tag{15c}$$

The relations for g_x and g_y are now reversed with respect to eq 12, if the values for *a*, *b*, and *c* are the same. Note that the Kramers pair of eq 11 cannot be related to that of eq 14 by a simple rotation of axes. Frequently, only the three *g*-values are given experimentally, not the corresponding axes. In Tables 2 to 4 the axes for the experimental *g*-values were chosen such that $g_z > g_y > g_x$, but they also could have been chosen such that $g_z > g_x > g_y$.

Scalar relativistic geometry optimizations were performed for the 6-coordinate low-spin Fe(III) porphyrins, where the axial ligands are either imidazole, pyrazole, or pyridine. In these scalar relativistic calculations we chose to distribute the hole in the electron configuration equally over five nearly degenerate orbitals, using fractional occupation numbers. These nearly degenerate orbitals closely resemble some porphyrin orbitals, which in D_{4h} symmetry would be labeled as a_{1u} (mainly p_z character of the porphyrin carbons not at the meso position), a_{2u} (mainly p_z character of the porphyrin carbons at the meso position, and p_z character of the porphyrin nitrogens), b_{2g} (mainly iron d_{xy}), and e_g (mainly d_{xz} and d_{yz}).

The geometry optimizations on the bis(imidazole), bis(pyrazole), and bis(pyridine) complexes were performed with different orientations of the planar axial ligands with respect to the porphyrin core. We carried out separate geometry optimizations with mutually parallel planes of the two axial ligands (∥) and with two mutually perpendicular planes (⊥), either with the planes of the two ligands positioned above the porphyrin nitrogens (over N_p) or with those planes positioned above the meso position of the porphyrin core (meso). For the bis(imidazole) and bis(pyrazole) complexes with two mutually parallel axial ligands the optimization was performed in C_{2v} and in C_{2h} symmetry, whereas in the two mutually perpendicular axial ligands the geometry of the complex was optimized in C_2 symmetry, with the added restriction that the porphyrin core has D_{2d} symmetry. For the bis(pyridine) complexes the symmetries are D_{2h} for parallel and D_{2d} for perpendicular axial ligands, respectively. In our calculations the ruffling of the core is largest if the two axial ligands are in two mutually perpendicular planes, particularly if the ligands lie over the meso position of the porphyrin core. This result is in accord with molecular mechanics calculations on similar systems.[10,19]

For the bis(imidazole) and the bis(pyrazole) complexes the optimized averaged FeN_p distance is approximately 2.00 Å, except when two mutually perpendicular axial ligands lie over the meso position. In that case the FeN_p distance is 1.978 Å, and the optimized FeN_{ax} distance, with N an imidazole nitrogen, is 1.959 Å for the bis(imidazole) complex and 1.949 Å for the bis(pyrazole) complex. In the other structures this distance between iron and the axial ligand is larger, namely in the order of 1.97−1.98 Å for the bis(imidazole) complex and 1.96−1.97 Å for the bis(pyrazole) complex. In Ref 17 several experimentally determined bond distances were summarized, including those for some bis(imidazole) iron−porphyrin complexes. Most of these bis(imidazole) complexes have an FeN_p distance on the order of 1.98−1.99 Å, and an FeN_{ax} distance of approximately 1.96−1.99 Å, not far from our calculated values.

For both the bis(imidazole) and the bis(pyrazole) complexes we did not find a strong preference for one of the orientations of the ligands: the calculated binding energies of the different complexes at the optimized geometries are all within 0.1 eV of each other. For the bis(pyridine) complex we find a preference for the complex with two mutually perpendicular pyridines over the meso position of the porphyrin ring. The energy of this structure is approximately 0.2−0.3 eV lower than that of the other structures. As for the related bis(imidazole) and the bis(pyrazole) structures with perpendicular ligands lying over the meso position, this bis(pyridine) structure also has the smallest FeN distances, namely an FeN_p distance of 1.969 Å and an FeN_{ax} distance of 1.993 Å. These distances can be compared with those derived from experiments for $[(TMP)Fe(4\text{-}NMe_2\ Py)_2]ClO_4$ and $[(TPP)Fe(Py)_2]ClO_4$, given in Ref 17. The pyridines in these complexes are nearly perpendicular over the meso position. The observed FeN_p distances are 1.964 Å and 1.982 Å, respectively, and the observed FeN_{ax} distances in these complexes range from 1.978 to 2.005 Å, close to the calculated values. For the bis(pyridine) complex with two mutually perpendicular pyridines we calculate an FeN_p distance of 1.987 Å and an FeN_{ax} distance of 2.023 Å. Both optimized structures with parallel pyridines have an FeN_p distance of 1.996 Å. The structure with the parallel planes over the meso position has an FeN_{ax} distance of 2.014 Å. For the one with the parallel planes over the porphyrin nitrogens this distance is 2.053 Å. Experimental results for $[(OEP)Fe(4\text{-}NMe_2\ Py)_2]ClO_4$,[17] which has two pyridines that are nearly parallel over the meso position, indicate

TABLE 2: Calculated *g*-Values of $[(P)Fe(ImH)_2]^+$ from ZORA Spin Restricted Frozen Core Calculations and Calculated Percentages of the Iron d Orbital Contributions to the Unpaired Electron[a]

	ligands	sign of $g_xg_yg_z$	g_x	g_y	g_z	$(d_{yz})^b$	$(d_{xz})^b$	(d_{xy}) or $(d_{x^2-y^2})^b$
AOC								
C_{2v}	∥ over N	+	1.78	2.16	2.59	96.7	2.5	0.7
C_{2h}	∥ over N	+	1.76	2.15	2.61	96.4	2.8	0.7
C_{2v}	∥ meso	+	2.04	1.57	2.93	92.0	6.9	1.1
C_{2h}	∥ meso	+	1.90	1.41	3.11	88.7	10.1	1.2
C_2	⊥ over N	−	0.31	0.33	3.85	49.5	49.0	1.5
C_2	⊥ meso	−	0.55	0.92	3.43	42.0	50.1	7.8
experiment[38−41]								
$[(PP)Fe(Im^-)_2]^-$			1.76	2.27	2.74	96.5	3.7	1.0
$[(TPP)Fe(N\text{-MeIm})_2]^+$			1.549	2.294	2.886	92.4	6.2	1.9
$[(PP)Fe(ImH)_2]^+$			1.55	2.25	2.92	92.3	6.5	1.7
$[(OEP)Fe(N\text{-MeIm})_2]^+$			1.506	2.273	2.986	92.1	7.3	2.0
$[(TPP)Fe(2\text{-MeImH})_2]^+$			0.82	1.87	3.41	78.1	18.8	3.1

[a] See footnote *a* of Table 1 for abbreviations. [b] See the text for the exact meaning of these percentages.

TABLE 3: Calculated *g*-Values of $[(P)Fe(Pz)_2]^+$ from ZORA Spin Restricted Frozen Core Calculations and Calculated Percentages of the Iron d Orbital Contributions to the Unpaired Electron[a]

	ligands	sign of $g_xg_yg_z$	g_x	g_y	g_z	$(d_{yz})^b$	$(d_{xz})^b$	(d_{xy}) or $(d_{x^2-y^2})^b$
AOC								
C_{2h}	∥ over N	+	1.88	2.16	2.32	98.7	0.8	0.4
C_{2v}	∥ over N	+	1.88	2.16	2.31	98.9	0.7	0.4
C_{2h}	∥ meso	+	2.12	1.86	2.44	97.8	1.6	0.5
C_{2v}	∥ meso	+	2.14	1.88	2.40	98.1	1.4	0.5
C_2	⊥ over N	−	0.16	0.41	3.75	46.4	52.3	1.4
C_2	⊥ meso	−	0.45	0.83	3.39	42.5	51.1	6.3
experiment [18,38,41]								
$[(TMP)Fe(3\text{-}NH_2Pz)_2]^+$			1.929	2.307	2.382	99.6	0.9	0.6
$[(TPP)Fe(3\text{-}NH_2Pz)_2]^+$			1.845	2.294	2.407	96.7	1.4	0.9
$[(TMP)Fe(3\text{-}CH_3Pz)_2]^+$			1.76	2.43	2.58	96.5	2.6	1.7
$[(TPP)Fe(3\text{-MePz})_2]^+$			1.739	2.382	2.581	95.5	2.7	1.6
$[(OEP)Fe(3\text{-MePz})_2]^+$			1.72	2.37	2.63	95.3	3.2	1.6

[a] See footnote *a* of Table 1 for abbreviations. [b] See the text for the exact meaning of these percentages.

TABLE 4: Calculated *g*-Values of $[(P)Fe(Py)_2]^+$ from ZORA Spin Restricted Frozen Core Calculations and Calculated Percentages of the Iron d Orbital Contributions to the Unpaired Electron[a]

	ligands	sign of $g_xg_yg_z$	g_x	g_y	g_z	$(d_{yz})^b$	$(d_{xz})^b$	(d_{xy}) or $(d_{x^2-y^2})^b$
AOC								
D_{2h}	∥ over N	+	1.50	1.99	2.98	90.9	8.0	1.1
D_{2h}	∥ meso	+	0.22	0.93	3.67	35.4	62.7	1.9
D_{2d}	⊥ over N	−	0.33	0.33	3.78	49.2	49.2	1.6
D_{2d}	⊥ meso	−	1.95	1.95	1.06	26.1	26.1	47.7
experiment [16−18,40]								
$[(TPP)Fe(4\text{-}NMe_2Py)_2]^+$			1.657	2.284	2.786	94.1	4.7	1.4
$[(OEP)Fe(4\text{-}NMe_2Py)_2]^+$			1.642	2.278	2.818	94.0	5.0	1.5
$[(TMP)Fe(4\text{-}NMe_2Py)_2]^+$			0.92	1.80	3.44	79.4	18.4	2.2
$[(TPP)Fe(Py)_2]^+$			−0.46	1.12	3.70	55.0	41.0	5.9
$[(TPP)Fe(4\text{-}CNPy)_2]^+$			2.63	2.63	0.96	8.1	8.1	80.4
$[(TMP)Fe(4\text{-}CNPy)_2]^+$			2.53	2.53	1.56	3.4	3.4	91.4

[a] See footnote *a* of Table 1 for abbreviations. [b] See the text for the exact meaning of these percentages.

an FeN_p distance of 2.002 Å and an FeN_{ax} distance of 1.995 Å, again not far from our calculated values.

Tables 2, 3, and 4 list the *g*-values calculated for the bis(imidazole), bis(pyrazole), and bis(pyridine) complexes, respectively. The results of the ZORA AOC calculations show trends that can also be observed in the experimental data. Unfortunately, in most of the work which reports the experimental *g*-values, the relative orientations of the axial ligands were not determined. This makes a comparison between theory and experiment less conclusive.

The results of the ZORA SCF calculations do not agree well with experiment and, therefore, we did not include them in the tables. The *g*-values calculated by this method are mostly of the large g_{max} type, with g_{max} in the order of 3−3.5, independent of the type of the axial ligands. When the two ligands lie perpendicular over the meso positions the results are different: the calculated *g*-values (ZORA SCF method) are all lower than the free electron g_e value. In this case the orbital energies of the orbitals which mostly resemble the iron d_{xz}, d_{yz}, and d_{xy} orbitals are close in energy, and the unpaired electron has mixed character comprising each of these orbitals.

In the ZORA AOC calculations we find a similar behavior of the calculated *g*-values when two pyridines lie perpendicular over the meso position. In that case we have an electron configuration somewhere between the usual $(d_{xy})^2(d_{xz},d_{yz})^3$ and the unusual $(d_{xz},d_{yz})^4(d_{xy})^1$ configuration for low-spin Fe(III) porphyrins. The fact that we now calculate *g*-values which are all lower than the free electron g_e-value is certainly not in line with any of the experiments. This discrepancy probably occurs because a multiconfigurational wave function would be required in this case, whereas our method works with single Slater determinants. The calculations do show, however, that the d_{xy}

orbital becomes more important, which is mainly because the porphyrin core is strongly ruffled. Because of this ruffling the four meso carbon atoms are displaced alternately above and below the porphyrin mean plane (D_{2d} ruffling). A second effect of this ruffling is that the pyrrole rings in the porphyrin are twisted by about 15° (calculated) out of the porphyrin mean plane.

The ruffling of the porphyrin core is stronger for pyridine ligands than for imidazole or pyrazole ligands because the pyridines, especially the α-hydrogens, interact more significantly with the porphyrin core. Depending on how large the ruffling is, the iron d_{xy} orbital may become higher in energy than the iron d_{xz} and d_{yz} orbitals, which leads to the unusual $(d_{xz},d_{yz})^4(d_{xy})^1$ electron configuration. A mechanism that can explain this effect was described in Ref 19 and is confirmed by the present calculations.

We also calculated the *g*-values in a planar porphyrin core with two pyridines lying perpendicular over the meso position. As for the similar situation with two imidazoles or two pyrazoles we find *g*-values of the large g_{max} type and small contributions of d_{xy} character in the unpaired electron. This again confirms that the ruffling of the porphyrin core increases the d_{xy} character of the unpaired electron. In Tables 2, 3, and 4 one also finds *g*-values of the large g_{max} type if the mutually perpendicular ligands are positioned above the porphyrin nitrogens (⊥ over N). In this case the ruffling of the core is not so large, and the unpaired electron consists mainly of the (almost) degenerate iron d_{xz} and d_{yz} orbitals. For the bis(pyridine) and bis(imidazole) complexes *g*-values of the large g_{max} type have been found. Our calculations suggest that we are then dealing with complexes with mutually perpendicular planes of the ligands. This confirms earlier studies based on experiments, see for example, Ref 17, where *g*-values of the large g_{max} type have been found for a complex with two (almost) perpendicular pyridines, and *g*-values of the rhombic type for a complex with two parallel pyridines.

Most experiments for the bis(pyrazole) and bis(imidazole) complexes give *g*-values of the normal rhombic type. In our calculation we find this type of *g*-values in two mutually parallel planes of the ligands, and they are in reasonable agreement with experimental values. In our ZORA AOC calculations we do not find any evidence for a $(d_{xz},d_{yz})^4(d_{xy})^1$ electron configuration for the bis(pyrazole) and bis(imidazole) complexes. Such an electron configuration is not excluded by Taylor's model if one only knows the principal values of the *g*-tensor and not its orientation, and it might be expected for the bis(pyrazole) complexes because of the closeness of the two largest *g*-values. We refer to Ref 31 for more details on this question and for experimental evidence of the usual $(d_{xy})^2(d_{xz},d_{yz})^3$ electron configuration for a bis(pyrazole) complex.

We calculate larger g_z values if the parallel planes lie over the meso position than if these parallel planes lie over the porphyrin nitrogens. The orbital energies of the iron d_{xz} and d_{yz} are closer in energy in the meso case, which increases the effect of spin−orbit coupling and leads to larger deviations from the free electron g_e-value. This effect is strongest for the bis(pyridine) complex.

In Figure 2 the effect of the orientation of the planes of the axial ligands on the calculated *g*-values is considered in more detail for the bis(imidazole) complex. In this figure calculated *g*-values are given for structures at ϕ-values intermediate between 0° and 90°. The structures were not optimized at each angle, but the geometries of the porphyrin ring and of the rotated axial ligands were interpolated linearly between the optimized structures at $\phi = 0°$, $\phi = 45°$, and $\phi = 90°$ that we discussed before. From the figure we can see that if the axial ligands remain parallel, the calculated *g*-values do not depend strongly on the actual angle ϕ. On the other hand, if the ligands are rotated in opposite directions, there is a stronger dependence, especially in the region close to 45°, which means close to a structure with perpendicular planes of the axial imidazoles. In this region we observe a sign change of at least one of the *g*-values. This can already be understood from the model by Taylor,[2] see eq 12, if we start with a situation that the iron d_{yz} character of the unpaired electron is large ($\phi = 0°$) and move to a situation where the d_{xz} and d_{yz} components are large and almost equal ($\phi = 45°$), and the d_{xy} contribution can be neglected. Note that there is some arbitrariness in the signs of the *g*-values, because only the sign of the product $g_x g_y g_z$ can be calculated. The signs in Figure 2 were chosen so that smooth curves resulted.

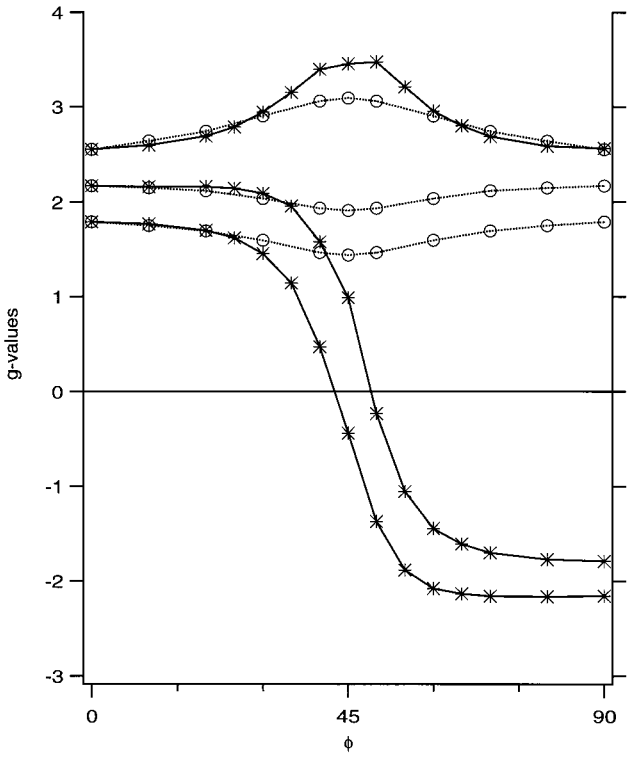

Figure 2. Effect of orientation of the imidazoles in $[(P)Fe(ImH)_2]^+$ on the calculated *g*-values. The three dotted lines represent the three *g*-values of two parallel axial imidazoles, each rotated with the same angle ϕ away from lying over the porphyrin nitrogens. Thus $\phi = 0°$ and $\phi = 90°$ correspond to C_{2v} (|| over N) and $\phi = 45°$ corresponds to C_{2v} (|| meso). The solid lines give the *g*-values if each imidazole is rotated in the opposite direction. Now $\phi = 0°$ still corresponds to C_{2v} (|| over N), but $\phi = 45°$ corresponds to C_{2v} (⊥ meso) and $\phi = 90°$ corresponds to C_{2h} (|| over N).

Another interesting effect is that when the two axial imidazoles remain parallel the orientation of the *g*-tensor strongly depends on the angle ϕ. At $\phi = 0°$ (axial ligands || over N) the principal axis with the smallest *g*-value lies in the plane of the axial ligands, whereas at $\phi = 45°$ (axial ligands || over meso position) the principal axis with the smallest *g*-value is perpendicular to the plane of the axial ligands (see Table 2). This is a nice illustration of the difference between eqs 12 and 15. Soltis and Strouse[32] observed this effect in experiments on two conformers of $[(TPP)Fe(ImH)_2]^+$. Theoretically this effect has been described by the concept of counterrotation of the *g*-tensor. (See Ref 21, for example.)

ZORA AOC vs ZORA SCF. For the low-spin iron complexes we observed that the ZORA SCF calculated *g*-values

often deviate (much) more from the free electron g_e value than the ones observed experimentally. This means that in the ZORA SCF calculation the effect of spin−orbit coupling for the unpaired electron is overestimated. The ZORA AOC calculated *g*-values are in better agreement with the experimental values than the ZORA SCF calculated values. From a theoretical point of view the ZORA SCF method is preferred over the ZORA AOC method, because in the latter method there is some arbitrariness in the construction of the AOC state and spin−orbit coupling is not included self-consistently. The latter point implies that the Hellmann−Feynman theorem, which is used implicitly in the derivation of the method used to calculate the *g*-tensor,[1] is no longer valid in the AOC method. Formally, this leads to the occurrence of some extra terms in the formulas for the *g*-tensor in the ZORA AOC method, but we ignored such terms.

We believe that the problems with the accuracy of the ZORA SCF calculations for the low-spin iron complexes, in comparison with experiment, are connected with the well-known problems of density functional calculations for open-shell molecules with nearly degenerate states. Consider, for example, the open-shell boron atom where self-consistent calculations with integer occupation numbers and present day density functionals (see for example Ref 33), may lead to nonspherical densities and nondegenerate orbitals which are not pure p orbitals. Similar problems arise for the $p_{1/2}$ and the $p_{3/2}$ orbitals in spin−orbit coupled equations. If our method for the calculation of the *g*-tensors is to be used, it would be preferable to have Kohn−Sham orbitals adapted to spherical symmetry. The use of fractional occupation numbers, as in the AOC method, is a possibility to ensure spherical densities and spherical Kohn−Sham potentials. In our iron−porphyrin complexes, where only Kramers degeneracy is present, the problem concerning the interaction with a small external magnetic field is not the same as the spatial degeneracy problem in the boron atom, of course, but also in these complexes there are nearly degenerate states and we believe that the problems are related.

Several improvements can still be made in the ZORA SCF calculations. First, one can take spin-polarization effects into account in the spin−orbit coupled equations, as suggested, for example, in Refs 34 and 35. Such spin-polarization effects generally will reduce the effect of spin−orbit coupling, which is precisely what is needed to improve the ZORA SCF results. However, the incorporation of spin-polarization effects in spin−orbit coupled equations is not straightforward and, therefore, these effects were not yet included. Moreover, the problems that we encountered in the example of the boron atom remain if spin-polarization effects are included. Still, spin-polarization effects may have the desired effect for the iron−porphyrin complexes.

Second, one may think, in principle, of improved density functionals that are better suited for the inclusion of the effects of spin−orbit coupling, because most of the present day density functionals result from nonrelativistic considerations.

Third, it is well-known that the Hohenberg−Kohn theorem no longer holds in the presence of a magnetic field. This means that one has to extend density functional theory to current density functional theory. Lee et al.,[36] for example, considered such effects in the calculation of nuclear shielding constants, but they found that the contributions of the current density functional to their calculated values were very small.

Finally, in addition to electronic effects, one has to consider nuclear motions as, for example, a rotation of the axial ligands over the porphyrin plane which may be important in model hemes and other vibrational effects.

In view of these findings, the ZORA AOC calculation may be considered as a suitable model that yields reasonable values for the *g*-tensor. The errors remaining in the ZORA SCF method are (partly) compensated by the approximations of the ZORA AOC method.

V. Conclusions

In agreement with experimental observations the *g*-values of low-spin iron porphyrins calculated with the ZORA AOC method are highly anisotropic. The simple model by Taylor,[2] in which the orbital of the unpaired electron consists only of (three) iron d orbitals, is still useful in the theoretical analysis if one adds ligand character of the same symmetry to the d orbitals of the unpaired electron. Our results are then well in line with the experimental analysis.

Optimization of the geometries of the various complexes gives iron−ligand distances in good agreement with the experimentally derived values. We confirm a mechanism, described in Ref 19, that strong ruffling of the porphyrin core of $[(P)Fe(Py)_2]^+$ can lead to the unusual $(d_{xz},d_{yz})^4(d_{xy})^1$ electron configuration, instead of the usual $(d_{xy})^2$ $(d_{xz},d_{yz})^3$ configuration for low-spin Fe(III) porphyrins.

For complexes with parallel planes of the axial ligands the *g*-values are rhombic whereas for axial ligands that are mutually perpendicular the *g*-values are almost always the large g_{max} type. This agrees with the experimental observations in Refs 10, 16−19.

References and Notes

(1) Lenthe, E. van; Wormer, P. E. S.; Avoird, A. van der *J. Chem. Phys.* **1997**, *107*, 2488.
(2) Taylor, C. P. S. *Biochim. Biophys. Acta* **1977**, *491*, 137.
(3) Zerner, M.; Gouterman, M.; Kobayashi, H. *Theor. Chim. Acta* **1966**, *6*, 363.
(4) Scheidt, W. R.; Chipman, D. M. *J. Am. Chem. Soc.* **1986**, *108*, 1163.
(5) Saito, M.; Kashiwagi, H. *Chem. Phys. Lett.* **1989**, *155*, 557.
(6) Rohmer, M.-M.; Dedieu, A.; Veillard, A. *Chem. Phys.* **1983**, *155*, 449.
(7) Jones, D. H.; Hinman, A. S.; Ziegler, T. *Inorg. Chem.* **1993**, *32*, 2092.
(8) Grodzicki, M.; Flint, H.; Winkler, H.; Walker, F. A.; Trautwein, A. T. *J. Phys. Chem. A* **1997**, *101*, 1352.
(9) Kuramochi, H.; Noodleman, L.; Case, D. A. *J. Am. Chem. Soc.* **1997**, *119*, 11442.
(10) Munro, O. Q.; Marques, H. M.; Debrunner, P. G.; Mohanrao, K.; Scheidt, W. R. *J. Am. Chem. Soc.* **1995**, *117*, 935.
(11) Rovira, C.; Ballone, P.; Parrinello, M. *Chem. Phys. Lett.* **1997**, *271*, 247.
(12) Harriman, J. E. *Theoretical Foundations of Electron Spin Resonance*; Academic Press: New York, 1978.
(13) Chang, Ch.; Pelissier, M.; Durand, Ph. *Phys. Scr.* **1986**, *34*, 394.
(14) Heully, J.-L.; Lindgren, I.; Lindroth, E.; Lundqvist, S.; Mårtensson-Pendrill, A.-M. *J. Phys. B* **1986**, *19*, 2799.
(15) Lenthe, E. van; Baerends, E. J.; Snijders, J. G. *J. Chem. Phys.* **1993**, *99*, 4597.
(16) Inniss, D.; Soltis, S. M.; Strouse, C. E. *J. Am. Chem. Soc.* **1988**, *110*, 5644.
(17) Safo, M. K.; Gupta, G. P.; Walker, F. A.; Scheidt, W. R. *J. Am. Chem. Soc.* **1991**, *113*, 5497.
(18) Safo, M. K.; Gupta, G. P.; Watson, C. T.; Simonis, U.; Walker, F. A.; Scheidt, W. R. *J. Am. Chem. Soc.* **1992**, *114*, 7066.
(19) Safo, M. K.; Walker, F. A.; Raitsimring, A. M.; Walters, W. P.; Dolato, D. P.; Debrunner, P. G.; Scheidt, W. R. *J. Am. Chem. Soc.* **1994**, *116*, 7760.
(20) Shokhirev N. V.; Walker, F. A. *J. Biol. Inorg. Chem.* **1998**, *3*, 581.
(21) Shokhirev N. V.; Walker, F. A. *J. Am. Chem. Soc.* **1998**, *120*, 981.
(22) Abragam, A.; Bleaney, B. *Electron Paramagnetic Resonance of Transition Ions;* Clarendon: Oxford, 1970.
(23) Baerends, E. J.; Ellis, D. E.; Ros, P. *Chem. Phys.* **1973**, *2*, 42.
(24) Velde, G. te; Baerends, E. J. *J. Comput. Phys.* **1992**, *99*, 84.

(25) Vosko, S. H.; Wilk, L.; Nusair, M. *Can. J. Phys.* **1980**, *58*, 1200.
(26) Becke, A. D. *Phys. Rev. A* **1988**, *38*, 3098.
(27) Perdew, J. P.; Wang, Y. *Phys. Rev. B* **1986**, *33*, 8800.
(28) Lenthe, E. van; Snijders, J. G.; Baerends, E. J. *J. Chem. Phys.* **1996**, *105*, 6505.
(29) Lenthe, E. van; Ehlers, A.; Baerends, E. J. *J. Chem. Phys.* **1999**, *110*, 8943.
(30) McGarvey, B. R. *Can. J. Chem.* **1975**, *53*, 2498.
(31) Raitsimring, A. M.; Borbat, P.; Shokhireva, T. K.; Walker, F. A. *J. Phys. Chem.* **1996**, *100*, 5235.
(32) Soltis, S. M.; Strouse, C. E. *J. Am. Chem. Soc.* **1988**, *110*, 2824.
(33) Baerends, E. J.; Branchadell, V.; Sodupe, M. *Chem. Phys. Lett.* **1997**, *265*, 481.
(34) Ramana, M. V.; Rajagopal, A. K. *Adv. Chem. Phys.* **1983**, *54*, 231.
(35) Wüllen, C. van *J. Chem. Phys.* **1995**, *103*, 3589.
(36) Lee, A. M.; Handy, N. C.; Colwell, S. M. *J. Chem. Phys.* **1995**, *103*, 10095.
(37) Hickman, D. L.; Shirazi, A.; Goff, H. M. *Inorg. Chem.* **1985**, *24*, 563.
(38) Walker, F. A.; Simonis, U. In Biological Magnetic Resonance, Vol. 12; *NMR of Paramagnetic Molecules*; Berliner, L. J., Rueben, J., Eds.; Plenum Press: New York, 1993; p 133.
(39) Chacko, V. P.; La Mar, G. N. *J. Am. Chem. Soc.* **1982**, *104*, 7002.
(40) Walker, F. A.; Reis, D.; Balke, V. L. *J. Am. Chem. Soc.* **1984**, *106*, 6888.
(41) Walker, F. A.; Huynh, B. H.; Scheidt, W. R.; Osvath, S. R. *J. Am. Chem. Soc.* **1986**, *108*, 5297.